EUROPEAN JOURNAL OF PURE AND APPLIED MATHEMATICS
2026, Vol. 19, Issue 2, Article Number 7279
ISSN 1307-5543 – ejpam.com
Published by New York Business Global

Stability Conditions, Bifurcation, and Chaos via the Euler Discretization of Van Der Pol-Duffing System

T. Alzkari[1,*], Monica Botros[2,3], W. W. Mohammed[4], A. B. Albidah[1], A. E. Matouk[1,5], T. N. Abdelhameed[6]

[1] *Department of Mathematics, College of Science Al-Zulfi, Majmaah University, Al-Majmaah, 11952, Saudi Arabia*
[2] *Basic Science Department, Faculty of Engineering, Delta University for Science and Technology, Gamasa, 11152, Egypt*
[3] *Faculty of Artificial Intelligence, Delta University for Science and Technology, Gamasa, Egypt*
[4] *Department of Mathematics, College of Science, University of Ha'il, Ha'il 2440, Saudi Arabia*
[5] *College of Engineering, Majmaah University, Al-Majmaah 11952, Saudi Arabia*
[6] *Mathematics Department, Faculty of Science, Beni-Suef University, Beni-Suef 62514, Egypt*

Abstract. The study of chaos and control in engineering oscillators has important applications in scientific and technological fields. In this work, the problem of investigating the discrete-time modified autonomous Van der Pol-Duffing oscillator based Euler discretization is considered. A circuit design of the proposed discrete-time system is presented via MATLAB Simulink. The system has one origin and two non-origin fixed points whose conditions for local stability are derived. The Neimark–Sacker bifurcation is shown around the non-zero fixed points when using a specific selection of the parameter values. Chaotic dynamics in the considered discrete-time system are illustrated by plotting the bifurcation diagram and the maximal Lyapunov exponents. The interesting multistability phenomenon is shown in this system, such as the coexistence of two period-1, period-2, period-4, and period-5 limit cycles. In addition, the coexistence of two one-band chaotic attractors is shown. Therefore, the corresponding basin sets of attraction are plotted to investigate this interesting type of multistability phenomenon, which results in higher complexity and unpredictability in the proposed discrete-time engineering model. Finally, the considered discrete-time system is stabilized at all its fixed points using a linear control method. Moreover, it is found that controlling chaos in the considered discrete-time system to one of the non-origin fixed points is faster when the initial data are located near one of the coexisting chaotic attractors than when they are chosen near the other.

2020 Mathematics Subject Classifications: 34C23, 34C28, 34D45, 37G10
Key Words and Phrases: The MAVPDO, euler discretization, stability conditions, neimark–Sacker bifurcation, coexistence of multi attractors, chaos control

---

*Corresponding Author.
DOI: https://doi.org/10.29020/nybg.ejpam.v19i2.7279

Email addresses: t.alzkari@mu.edu.sa (T. Alzkari), monica.botros@deltauniv.edu.eg (M. Botros), w.mohammed@uoh.edu.sa (W. W. Mohammed), a.albedah@mu.edu.sa (A. B. Albidah) ae.mohamed@mu.edu.sa (A. E. Matouk), t.ahmed@mu.edu.sa (T. N. Abdelhameed)

1. Introduction

Exploring the nonlinear dynamics of discrete-time dynamical systems (DTDS) is considered to be an interesting research topic [1]. Many models related to science, engineering, and economics can be described in terms of DTDS [2–7] because of their efficiency in providing more convenient tools for describing processes that evolve over non-overlapping intervals or which have different time scales. In addition, DTDS require less computational complexity than the corresponding continuous-time counterparts. Furthermore, the DTDS always show a variety of rich dynamical behaviors, including bifurcations, chaos, and the multistability dynamical phenomenon. Euler's method is considered one of the most powerful tools for discretizing continuous dynamical systems. It helps to improve the calculations in numerical schemes and offers distinct stability properties. In addition, it is essential in optimization, stochastic simulation, and applications to the dynamics of rigid body since it supports structures-preserving techniques that preserve physical invariants such as momentum and energy. So, the Euler discretization method plays an important role in obtaining discrete integrators in continuous dynamical systems. For example, George et al. [8] investigated the bifurcations in a discretized SIR epidemic model based on the Euler scheme; Al-Basyouni and Khan [9] applied the Euler forward formula to display chaos and bifurcations from a COVID-19 epidemic model, and Guiying and Rudidi [10] investigated the complex dynamics in Lorenz system and Holling-Tanner system using the Euler method.

The modified autonomous Van der Pol-Duffing oscillator (MAVPDO) was modeled by Matouk and Agiza in 2008 [11]. The MAVPDO has a unique nonlinear term with cubic nonlinearity, which attracts many scientists to investigate its dynamical behaviors and shows potential applications in engineering field [12–20].

To demonstrate the novelty in this work, we will summarize the key findings of this study as follows: The MAVPDO's system is discretized based the on Euler's method. The engineering meaning of the discretized system is explained by designing the corresponding circuit via MATLAB Simulink. Some dynamical analysis of the considered discrete-time system is discussed such as the local stability of all the system's fixed points and the N–S bifurcation conditions. Chaotic dynamics in the considered discrete-time system are also shown via the N–S bifurcation route. The interesting multistability phenomenon is shown in this system, such as the coexistence of two period-1, period-2, period-4, period-5 limit cycles (LCs) and two one-band chaotic attractors (CAs). The analytical results are accompanied with numerical simulations such as maximal Lyapunov exponents (MLEs) and bifurcation diagrams, phase plots, and basin of attractions, which verify the occurrence of complex dynamics in the considered discrete-time system. Controlling chaos in this system to all three of its fixed point is obtained via the linear feedback control scheme. In addition, it is found that controlling the discrete-time MAVPDO to one of the non-origin fixed points is faster when the initial data are located near to one of the coexisting chaotic attractors than when they are chosen near the other.

In conclusion, we will summarize the structure of the paper as follows: in Section 2, the description of the MAVPDO and its Euler discretization are fully explained. In Section 3, the local stability conditions of the three fixed points of the discretized MAVPDO are discussed. In Section 4, some conditions for the existence of the N–S bifurcation in the discretized MAVPDO are shown. In Section 5, various numerical tools are applied to the considered discrete-time system. In Section 6, the discretized MAVPDO system is stabilized to its three fixed points using linear control. In Section 7, the concluding part of this work and the future works are discussed.

2. Description of the chaotic MAVPDO system and its discretization

The Multisim circuit realization of the MAVPDO is obtained by using TL074 operational amplifiers (OA), analogue incorporating AD633 multipliers, and essential circuit elements, including capacitors and resistors, the circuit implementation of the unique 3D system is laid out as follows. Compare this to our system, these electronic components' values are presented as

$$\begin{aligned} R_1 &= R_2 = R_3 = R_4 = R_9 = R_{10} = R_{12} = 100K\Omega,\ R_5 = 0.5K\Omega, \\ R_6 &= R_8 = 1K\Omega,\ R_7 = 10K\Omega,\ R_{11} = 59.523K\Omega,\ C_1 = C_2 = C_4 = 10nF. \end{aligned}$$

So, the dimensionless equations are

$$\begin{aligned} \frac{dx}{dt} &= \frac{1}{R_6C_2}x^3 - \frac{1}{R_7C_2}x - \frac{1}{R_8C_2}y, \\ \frac{dy}{dt} &= -\frac{1}{R_1C_1}x + \frac{1}{R_{11}C_1}y + \frac{1}{R_4C_1}z, \\ \frac{dz}{dt} &= -\frac{1}{R_5C_4}y. \end{aligned}$$

whose circuit's implementation is illustrated in figure 1.

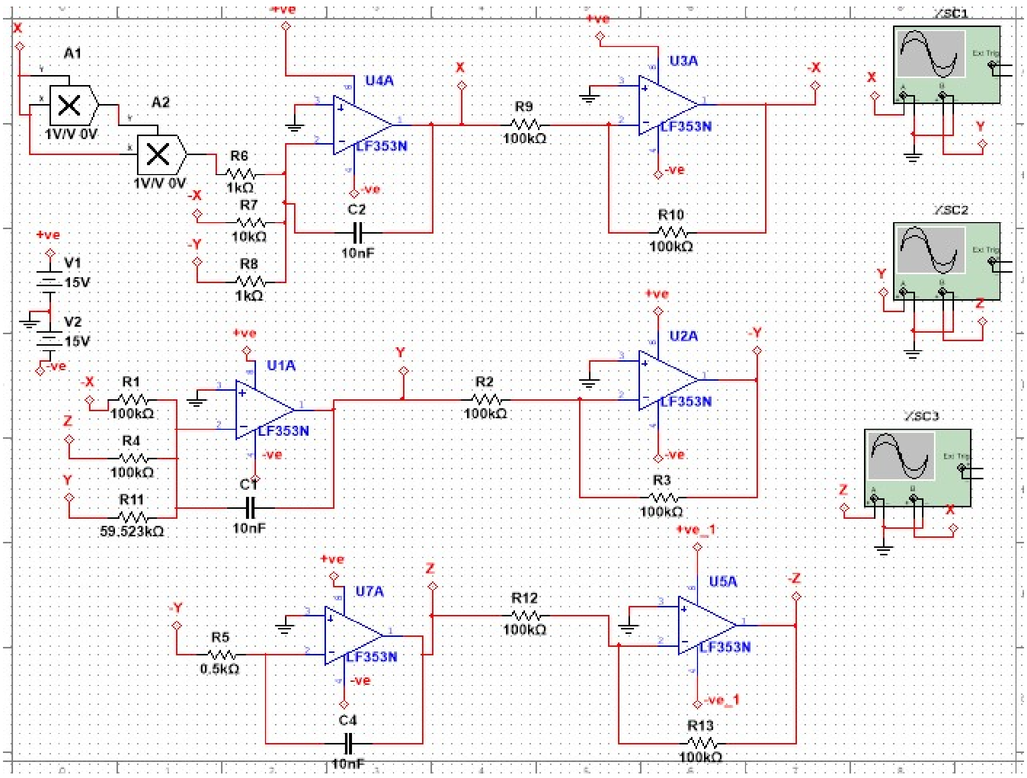

Figure 1: The proposed circuit schematics by Multisim, corresponding to the values of parameters showed above.

The rescaled MAVPDO is represented by

$$
\begin{aligned}
\frac{dx}{dt} &= -\nu x^3 + \mu\nu x + \nu y, \\
\frac{dy}{dt} &= x - (z + \alpha y), \\
\frac{dz}{dt} &= \beta y,
\end{aligned} \tag{1}
$$

which can be considered as a modification to the Van der Pol-Duffing oscillator [21]. The chaotic attractors can experimentally be obtained when from the above-mentioned circuit, as shown in figure 2.

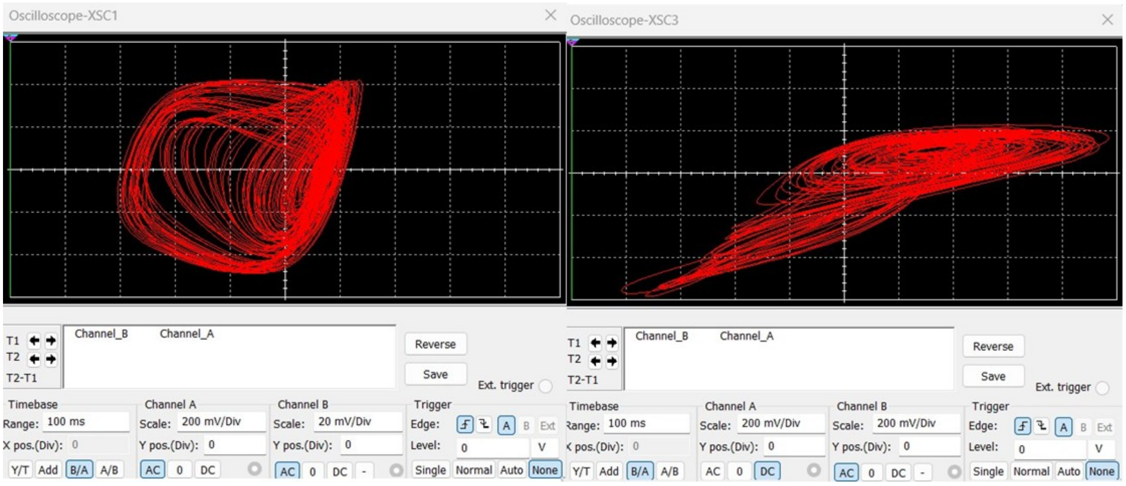

Figure 2: Chaotic dynamics of circuit implementation of the MAVPDO *(1)* simulated by Multisim at $\alpha = 1.68$

Applying Euler method to system *(1)*, we obtain the following discrete-time model

$$\begin{aligned} x_{m+1} &= x_m + h\left(-\nu x_m^3 + \mu\nu x_m + \nu y_m\right), \\ y_{m+1} &= y_m + h\left(x_m - (z_m + \alpha y_m)\right), \\ z_{m+1} &= z_m + h\beta y_m, \end{aligned} \tag{2}$$

where $m \in N$ and h represents the time step. According to Refs. [11], the system *(2)* is linearizable and has the three fixed points:

$$\overline{P}_0 = (0,0,0) \text{ and } \overline{P}_\pm = (\pm\sqrt{\mu}, 0, \pm\sqrt{\mu}). \tag{3}$$

Using Simulink to represent the continuous and discrete nonlinear dynamical systems *(1)* and *(2)* with three variables, x, y, and z, each obtained through an integrator block, are shown in figures 1 and 2. For the continuous system *(1)*, the derivatives are computed using combinations of summation, gain, and product blocks, introducing both linear and nonlinear coupling between variables. Adjustable gain blocks ($\alpha = a$ (in Simulink) $=$ 4.2, $\beta = b$ (in Simulink) $= 200$, $\mu = u$ (in Simulink) $= 100$, $\mu\nu = uv$(in Simulink) $=$ 10) define key parameters controlling the system's behavior, which can range from stable motion to chaotic dynamics. For the discrete system *(2)*, there are parameters added to the discrete time, its values affect the behavior of the generator, where the step size of the solver is presented as an actual component, and the delay unit used in the model has two parameters; the delay time (D) in seconds, and the initial value (IV) which represents the initial state of the dynamical system.

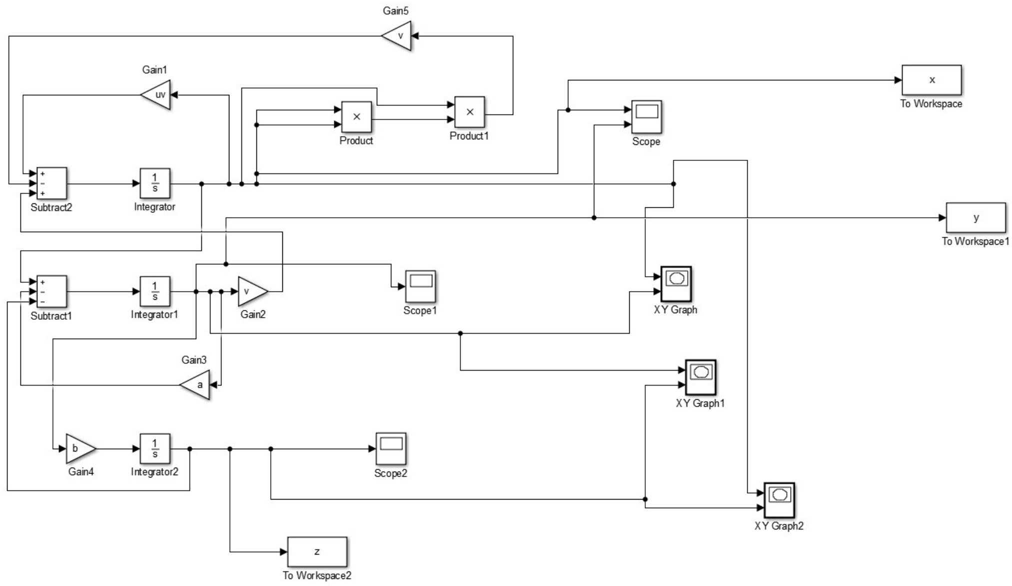

Figure 3: Circuit realization of the continuous-time model *(1)* using Simulink.

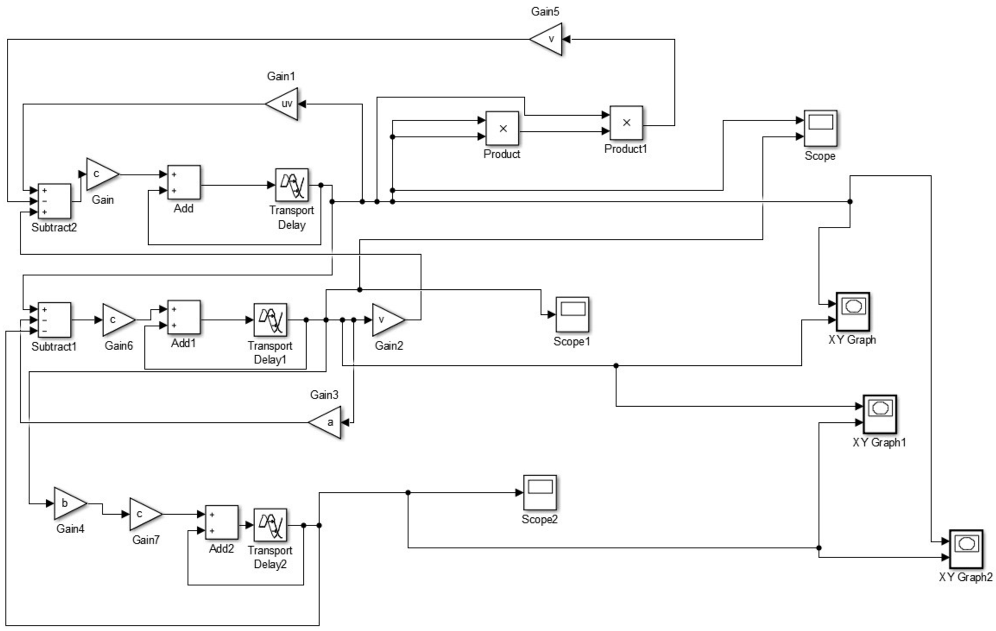

Figure 4: Circuit realization of the discrete-time model *(2)* using Simulink.

3. Local stability

System *(2)* has the following Jacobian matrix

$$J(x,y,z)=\begin{bmatrix} 1-vh\left(3x^2-\mu\right) & vh & 0 \\ h & -\alpha h+1 & -h \\ 0 & h\beta & 1 \end{bmatrix}. \tag{4}$$

Assume that the characteristic equation of *(4)* has the form

$$\lambda^3+\xi_1\lambda^2+\xi_2\lambda+\xi_3=0. \tag{5}$$

Remark 3.1 For a DTDS, a fixed point $\overline{P}$ is locally asymptotically stable (LAS) if $|\lambda_i|<1 \forall i=1,2,3$ and unstable if $\exists\lambda_i, |\lambda_i|>1$. In addition $\overline{P}$, is unstable (source) if $|\lambda_i|>1$ and unstable (saddle) if $|\lambda_i|>1$ and $|\lambda_j|<1$ for some $i\neq j$.

Remark 3.2 a fixed point $\overline{P}$ is LAS (or sink) if all the properties mentioned below are met [5],

$$\begin{aligned} (i)\,1+\xi_1+\xi_2+\xi_3 &> 0, \quad (ii)\,1-\xi_1-\xi_3+\xi_2>0, \\ (iii)\,1-\left(\xi_3^2+\xi_2\right)+\xi_1\xi_3 &> 0, \quad (iv)\,\xi_2>\xi_1\xi_3+\xi_3^2-1. \end{aligned}$$

According to the conditions (i)-(iv), the local stability of the fixed points $\overline{P}_0$, $\overline{P}_+$ and $\overline{P}_-$ is determined by the coefficients ξ_1, ξ_2 and ξ_3. They are given as follows:

For $\overline{P}_0$,

$$\begin{aligned} \xi_1 &= -\left(3+h\left(\mu\nu-\alpha\right)\right), \\ \xi_2 &= 3-h\left[\nu h+h\alpha\mu\nu-h\beta+2\left(\alpha-\mu\nu\right)\right], \\ \xi_3 &= -1+h\left[\nu h+h\beta+\alpha+\mu\nu\left(-\beta h^2+\alpha h-1\right)\right]. \end{aligned}$$

For $\overline{P}_\pm$,

$$\begin{aligned} \xi_1 &= -\left(3+h\left(2\mu\nu+\alpha\right)\right), \\ \xi_2 &= 3-h\left[\nu h\left(1-2\alpha\mu\right)-h\beta+2\left(\alpha+2\mu\nu\right)\right], \\ \xi_3 &= -1+h\left[\alpha+h\left(v-\beta\right)+2\mu\nu\left(\beta h^2-\alpha h+1\right)\right]. \end{aligned}$$

4. Existence of N–S bifurcation around the non-origin fixed points

For $\beta=200$, $v=100$, $\mu=0.1$, and $h=0.01$ the non-origin fixed points $\overline{P}_{+,-}$ satisfy the eigenvalue criterion of the N–S bifurcation [22] at $\alpha_c^{(NS)}=5.42468831$. When $\alpha>\alpha_c^{(NS)}$ all the stability conditions (i)-(iv) hold, which imply that $\overline{P}_{+,-}$ are LAS. When $\alpha<\alpha_c^{(NS)}$ all the fixed points are unstable. Moreover, $\overline{P}_{+,-}$ change from sink to saddle as crosses α the critical value $\alpha_c^{(NS)}$.

We will examine the N–S bifurcation type in the rest of this section. Firstly, we define the vector represents the system's state variable X. We specify the change of variables $(X, a) = \left(X - \overline{X}, \alpha - \alpha^{(N)}\right)$, to transform the non-origin fixed points $\overline{P}_{+,-}$ to the zero fixed point $\overline{P}_0$. Thus, the transformed system version of system *(2)* is read as:

$$X_{n+1} = F\left(X_n, \alpha\right). \tag{6}$$

The system *(6)* becomes

$$X_{n+1} = JX_n + \frac{1}{2!}B\left(X_n, X_n\right) + \frac{1}{3!}C\left(X_n, X_n, X_n\right) + o\left(\|X_n\|^4\right), \tag{7}$$

where

$$\begin{aligned} B_i\left(x, y\right) &= \sum_{j,k=1}^{n} \left.\frac{\partial^2 F_i\left(\xi, 0\right)}{\partial \xi_j \partial \xi_k}\right|_{\xi=0} x_j y_k, \\ C_i\left(x, y, z\right) &= \sum_{j,k,m=1}^{n} \left.\frac{\partial^3 F_i\left(\xi, 0\right)}{\partial \xi_j \partial \xi_k \partial \xi_m}\right|_{\xi=0} x_j y_k z_m, \quad i = 1, 2, 3. \end{aligned} \tag{8}$$

If $\overline{P}_0$ exhibits a N–S bifurcation, then $J\left(\alpha_c^{(NS)}\right)$ has two eigenvalues of the form $\lambda_{1,2} = \lambda_{1,2}\left(\alpha_c^{(NS)}\right) = e^{\pm I\theta_0}$, $I = \sqrt{-1}$, $0 < \theta_0 < \pi$. The direction of bifurcation is determined by

$$l_1\left(0\right) = -\frac{\left|g_{11}\right|^2}{2} - \frac{\left|g_{02}\right|^2}{4} + Re\left(\frac{g_{21}e^{-I\theta_0}}{2}\right) - Re\left(g_{20}g_{11}\frac{e^{-2I\theta_0} - 2e^{-I\theta_0}}{2 - 2e^{I\theta_0}}\right) \tag{9}$$

where l_1 refers to the first Lyapunov coefficient [23],

$$\begin{aligned} g_{20} &= \langle \sigma, B\left(\rho, \rho\right)\rangle, \ g_{11} = \langle \sigma, B\left(\rho, \overline{\rho}\right)\rangle, \ g_{02} = \langle \sigma, B\left(\overline{\rho}, \overline{\rho}\right)\rangle, \\ g_{21} &= \langle \sigma, C\left(\rho, \rho, \overline{\rho}\right)\rangle + 2\left\langle \sigma, B\left(\rho, \left(I_3 - J\right)^{-1}\right) B\left(\rho, \overline{\rho}\right)\right\rangle + \left\langle \sigma, B\left(\overline{\rho}, \left(e^{2I\theta_0}I_3 - J\right)^{-1}\right) B\left(\rho, \rho\right)\right\rangle \\ &\quad + \frac{e^{-I\theta_0} - 2}{1 - e^{I\theta}}g_{20}g_{11} - \frac{2}{1 - e^{-I\theta_0}}\left|g_{11}\right|^2 - \frac{e^{I\theta_0}}{e^{3I\theta} - 1}\left|g_{02}\right|^2, \end{aligned}$$

and I_3 is an identity matrix. The vectors $\sigma \in C^3$ and $\rho \in C^3$ must satisfy

$$\begin{aligned} J\left(\alpha_c^{(NS)}\right)\rho &= e^{I\theta_0}\rho, \ J\left(\alpha_c^{(NS)}\right)\overline{\rho} = e^{-I\theta_0}\overline{\rho}, \ J^T\left(\alpha_c^{(NS)}\right)\sigma = e^{-I\theta_0}\sigma, \\ J^T\left(\alpha_c^{(NS)}\right)\overline{\sigma} &= e^{I\theta_0}\overline{\sigma}, \ \langle \sigma, \rho\rangle = \overline{\sigma}^T\rho = 1. \end{aligned} \tag{10}$$

Theorem 1. The system *(2)* exhibits subcritical N–S bifurcation around $\overline{P}_{+,-}$ using $\beta = 200$, $v = 100$, $\mu = 0.1$, $h = 0.01$ and $\alpha_c^{(NS)} = 5.42468831$. Therefore, unstable invariant closed curves bifurcates from $\overline{P}_{+,-}$, while these fixed points change from unstable to stable as α crosses $\alpha_c^{(NS)}$.

Proof: The Jacobian matrix *(4)* evaluated at $\overline{P}_{+,-}$ using the parameter values $\beta = 200$, $v = 100$, $\mu = 0.1$, $h = 0.01$ and the critical parameter $\alpha_c^{(NS)} = 5.42468831$ is given by

$$J\left(\overline{P}_{+,-}\right) = \begin{pmatrix} 0.8 & 1 & 0 \\ 0.01 & 0.9457531168 & -0.01 \\ 0 & 2 & 1 \end{pmatrix}, \tag{11}$$

with the eigenvalues $\lambda_{1,2} = 0.9915753117 \pm 0.12953146682I$, $\lambda_3 = 0.7626024935$ and the corresponding eigenvectors

$$\begin{aligned} \rho &= (0.1228781924 + 0.3243795669I, 0.06555778952 + 0.04622652416I, \\ &\quad -0.7763009449 + 0.9617391626I)^T, \\ \sigma &= (0.4964419915 + 0.1302315022I, 7.823695 + 8.925400124I, \\ &\quad -0.6470316495 + 0.6460823076I)^T, \end{aligned} \tag{12}$$

which fulfils the property *(10)*. Hence, the multi-linear functions B, C are obtained as follows

$$B(\xi,\eta) = \begin{pmatrix} -1.897366596\xi_1\eta_1 \\ 0 \\ 0 \end{pmatrix}, \; C(\xi,\eta,\zeta) = \begin{pmatrix} -6\xi_1\eta_1\zeta_1 \\ 0 \\ 0 \end{pmatrix}.$$

Now, the quantities g_{ij} appearing in Eq. *(9)* are obtained as follows

$$\begin{aligned} g_{20} &= 0.03418060048 - 0.04206996578I, \; g_{11} = -0.05347528783 + 0.008865047208I, \\ g_{02} &= 0.04592761108 + 0.02878975531I, \; g_{21} = 0.2673437878 + 0.3178921752I. \end{aligned} \tag{13}$$

Inserting Eq. *(13)* into Eq. *(9)*, yields $l_1(0) = 0.1405739367 > 0$ which refers to emergence of unstable invariant closed curves around $\overline{P}_{+,-}$.

On the other hand, when the parameter values are fixed at $\alpha = 4$, $\beta = 200$, $v = 100$, $\mu = 0.1$, the N–S bifurcation around the non-origin fixed points $\overline{P}_{+,-}$ is found at the critical value $h = 0.002563830238$, which satisfies the eigenvalue criterion of the N–S bifurcation [22]. This illustrates the extent to which changing the step size parameter can affect the N–S bifurcation points in the discrete-time system *(2)*. In addition, the previous results are consistent with Ref. [11], which showed the presence of Hopf bifurcation in the continuous system *(1)* at the same previous parameter values but with a change in α to 3.5078.

5. Coexistence of periodic orbits and chaotic attractors

In this Section, the parameter values $\beta = 200$, $v = 100$, $\mu = 0.1$ and $h = 0.01$ are fixed, while the dynamical parameter α is varied. The related bifurcation diagram and computation of MLEs are illustrated in figures 3 and 4.

Coexistence of period- 1, 2, 4, 5 LCs are observed around $\overline{P}_+$ and $\overline{P}_-$ when $\alpha = 5, 4.8, 4.68$ and 4.6, respectively. In addition, Coexistence of one-band chaos is observed around $\overline{P}_+$ and $\overline{P}_-$ when $\alpha = 4.4$. In figures 5 to 9, the previous results are depicted, along with computing the basin sets of attraction (BSA), For example; In Fig. 5c, the blue region refers to a self-excited attractor (SEA) connected with LC around $\overline{P}_-$, the red region refers to a SEA connected with LC around $\overline{P}_+$, the turquoise region refers to a period-1 LC around $\overline{P}_+$ and the yellow region refers to a period-1 LC around $\overline{P}_-$. In Fig. 6c, the blue region refers to a quasi-periodic attractor around $\overline{P}_0$, the red region refers to another quasi-periodic attractor around $\overline{P}_0$, the turquoise region refers to a period-2 LC around $\overline{P}_+$ and the yellow region refers to a period-2 LC around $\overline{P}_-$. In Fig. 7c, the blue region refers to a quasi-periodic attractor around $\overline{P}_0$, the red region refers to another quasi-periodic attractor around $\overline{P}_0$, the turquoise region refers to a period-4 LC around $\overline{P}_+$ and the yellow region refers to a period-4 LC around $\overline{P}_-$. In Fig. 8c, the blue region refers to a quasi-periodic attractor around $\overline{P}_0$, the red region refers to another quasi-periodic attractor around $\overline{P}_0$, the turquoise region refers to a period-5 LC around $\overline{P}_+$ and the yellow region refers to a period-5 LC around $\overline{P}_-$. In Fig. 9c, the blue region refers to a quasi-periodic attractor around $\overline{P}_0$, the red region refers to another quasi-periodic attractor around $\overline{P}_0$, the turquoise region refers to a one-band chaos around $\overline{P}_+$ and the yellow region refers to a one-band chaos around $\overline{P}_-$. Furthermore, double-band CA is found when $\alpha = 4$ (See figure 10).

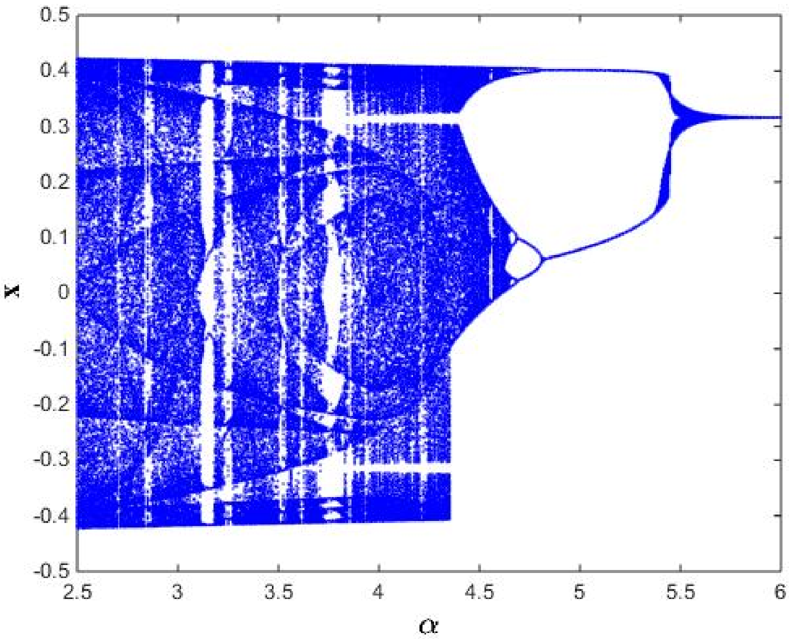

Figure 5: The bifurcation diagram of system *(2)* as α is varied.

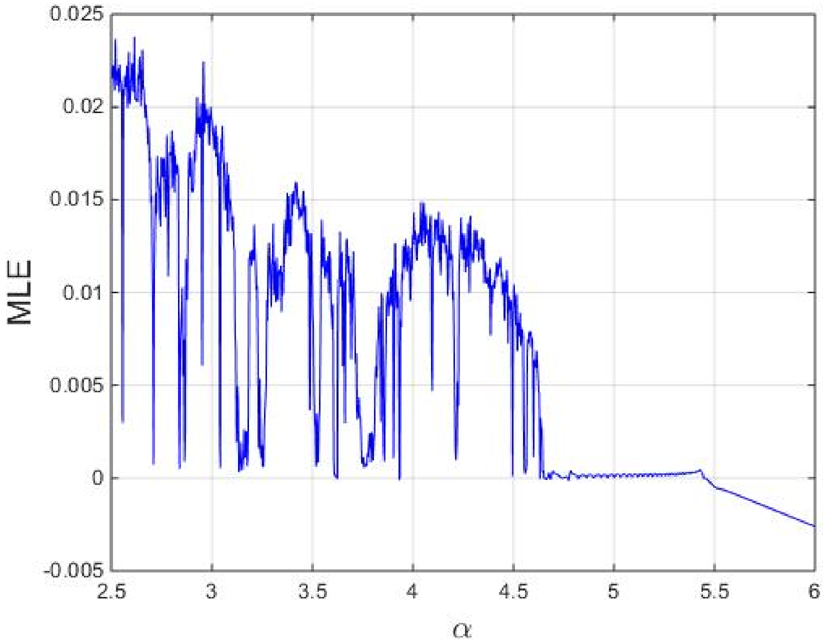

Figure 6: The MLEs of system *(2)* as α is varied.

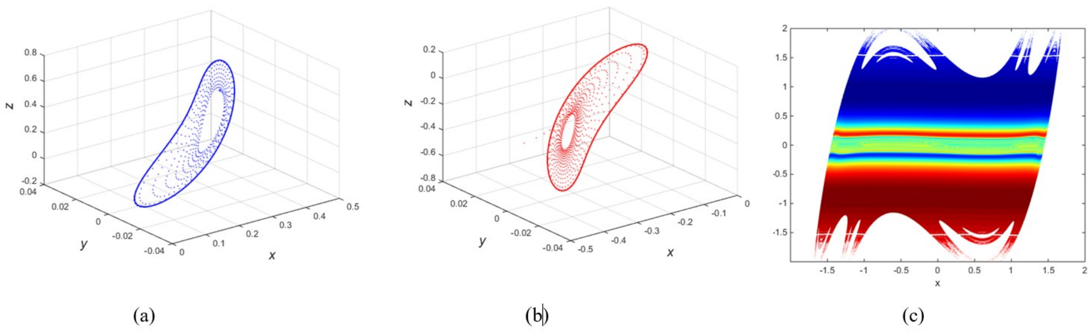

Figure 7: For $\alpha = 5$, system *(2)* shows: (a) a period-1 LC surrounding $\overline{P}_+$ when $(x_0, y_0, z_0) = (0.4, 0.01, 0.4)^T$, (b) a period-1 LC surrounding $\overline{P}_-$ when $(x_0, y_0, z_0) = (-0.4, 0.01, -0.4)^T$, and (c) the corresponding BSA. *(*

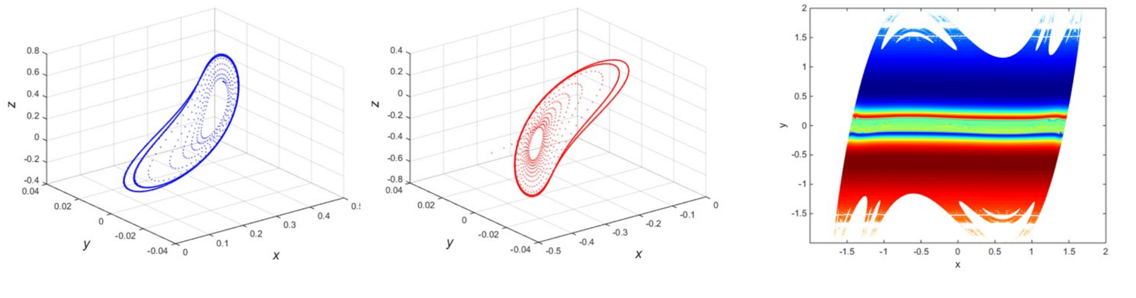

(a) (b) (c)

Figure 8: For $\alpha = 4.8$, system *(2)* shows: (a) a period-2 LC surrounding $\overline{P}_+$ when $(x_0, y_0, z_0) = (0.4, 0.01, 0.4)^T$, (b) a period-2 LC surrounding $\overline{P}_-$ when $(x_0, y_0, z_0) = (-0.4, 0.01, -0.4)^T$, and (c) the corresponding BSA.

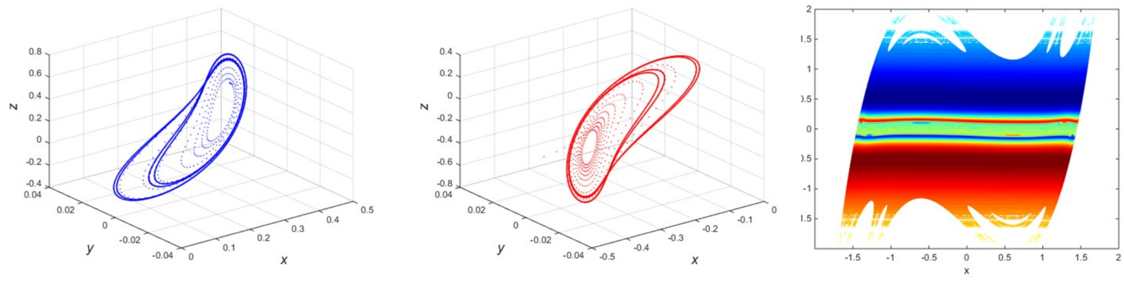

(a) (b) (c)

Figure 9: For $\alpha = 4.68$, system *(2)* shows: (a) a period-4 LC surrounding $\overline{P}_+$ when $(x_0, y_0, z_0) = (0.4, 0.01, 0.4)^T$, (b) a period-4 LC surrounding $\overline{P}_-$ when $(x_0, y_0, z_0) = (-0.4, 0.01, -0.4)^T$, and (c) the corresponding BSA.

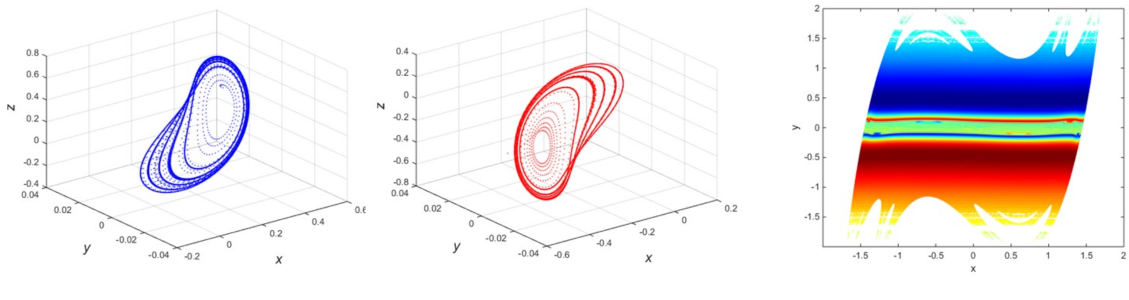

(a) (b) (c)

Figure 10: For $\alpha = 4.6$, system *(2)* shows: (a) a period-5 LC surrounding $\overline{P}_+$ when $(x_0, y_0, z_0) = (0.4, 0.01, 0.4)^T$, (b) a period-5 LC surrounding $\overline{P}_-$ when $(x_0, y_0, z_0) = (-0.4, 0.01, -0.4)^T$, and (c) the corresponding BSA.

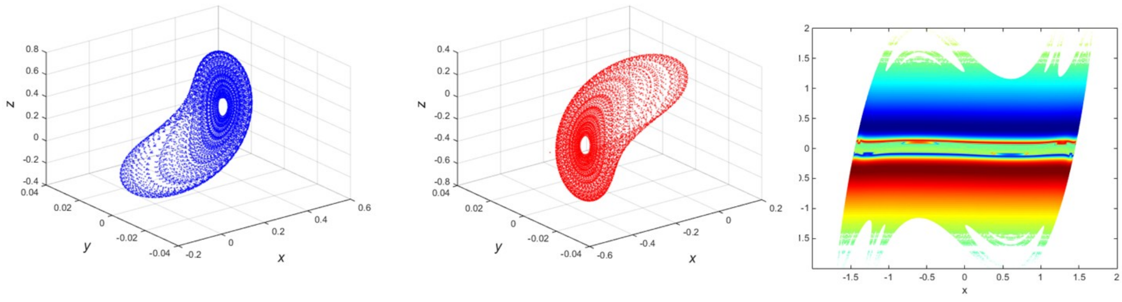

(a) (b) (c)

Figure 11: For $\alpha = 4.4$, system *(2)* shows: (a) a one-band chaos around $\overline{P}_+$ when $(x_0, y_0, z_0) = (0.4, 0.01, 0.4)^T$, (b) a one-band chaos around $\overline{P}_-$ when $(x_0, y_0, z_0) = (-0.4, 0.01, -0.4)^T$, and (c) the corresponding BSA.

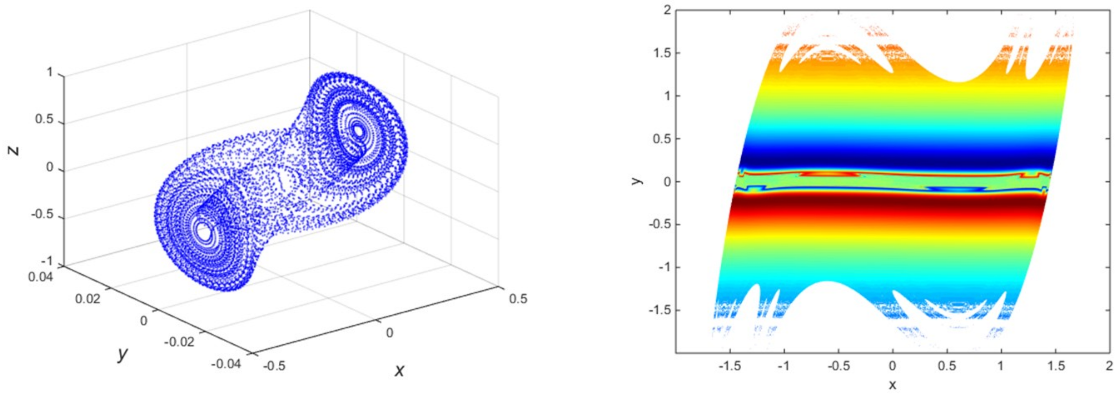

(a) (b)

Figure 12: For $\alpha = 4$, system *(2)* shows: (a) a double-band chaos when $(x_0, y_0, z_0) = (0.4, 0.01, 0.4)^T$, and (b) the corresponding BSA.

On the other hand, another route of complex dynamics starting from the N–S bifurcation to chaos is obtained by changing the step size parameter h and fixing the other parameter values at $\alpha = 4$, $\beta = 200$, $v = 100$, $\mu = 0.1$. This scenario is depicted in figure 11 and the corresponding MLEs are shown in figure 12.

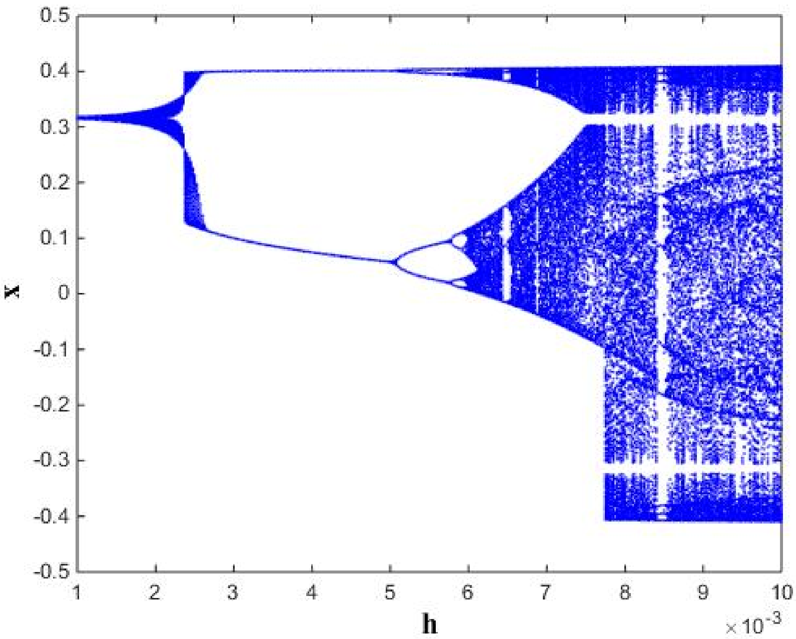

Figure 13: The bifurcation diagram of system *(2)* as h is varied.

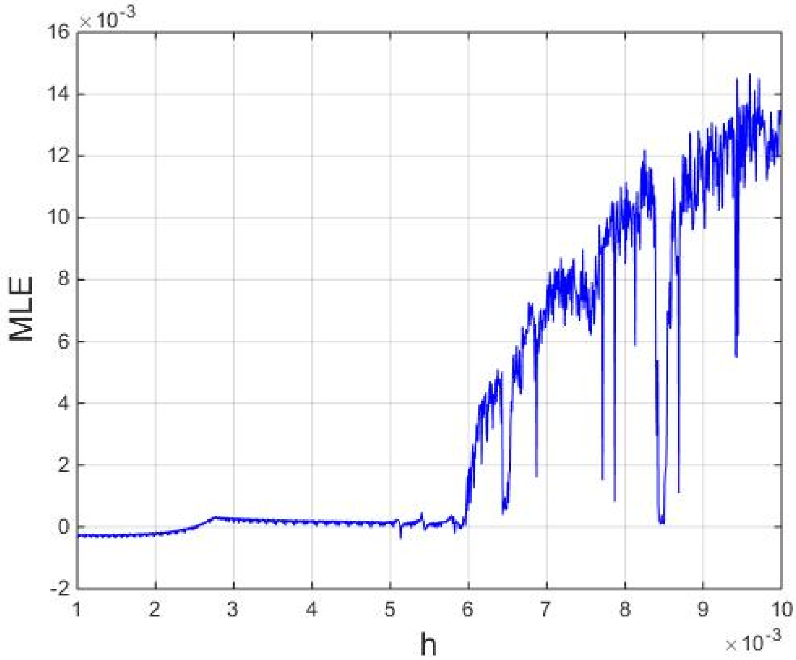

Figure 14: The MLEs of system *(2)* as h is varied.

6. Chaos control of system *(2)*

The controlled version of system *(2)* is described by

$$\begin{aligned} x_{m+1} &= x_m + h\left(-\nu x_m^3 + \mu\nu x_m + \nu y_m\right) - K_1\left(x_m - \overline{P}_x\right), \\ y_{m+1} &= y_m + h\left(x_m - (z_m + \alpha y_m)\right) - K_2\left(y_m - \overline{P}_y\right), \\ z_{m+1} &= z_m + h\beta y_m - K_3\left(z_m - \overline{P}_z\right), \end{aligned} \tag{14}$$

where $\left(\overline{P}_x, \overline{P}_y, \overline{P}_z\right)$ is an arbitrary fixed point of the discrete-time MAVPDO *(2)* and $K_i \geq 0$, $i = 1, 2, 3$ are feedback control gains (FCGs) that are designed to satisfy the stability criterion in Remarks 3.1 and 3.2. It is found that when the parameter values $\alpha = 4$, $\beta = 200$, $v = 100$, $\mu = 0.1$ and $h = 0.01$ are selected, the suitable FCGs that stabilize system *(14)* to one of the fixed points $\overline{P}_0$, $\overline{P}_+$ and $\overline{P}_-$, can be chosen as $K_1 = 1$, $K_2 = 0$, and $K_3 = 0$. The numerical results are outlined in figures 13 to 15, in which the initial conditions $(x_0, y_0, z_0) = (0, 0.01, 0)^T$ are used.

On the other hand, when the parameter values $\alpha = 4.4$, $\beta = 200$, $v = 100$, $\mu = 0.1$, and $h = 0.01$ are selected, it is found that controlling the discrete-time MAVPDO *(14)* to one of the non-origin fixed points is faster when the initial data are located near to one of the coexisting chaotic attractors than when they are chosen near the other. The results are depicted in figures 16 and 17, in which the blue and red attractors represent the attractors given in Figs. 9a and 9b, respectively.

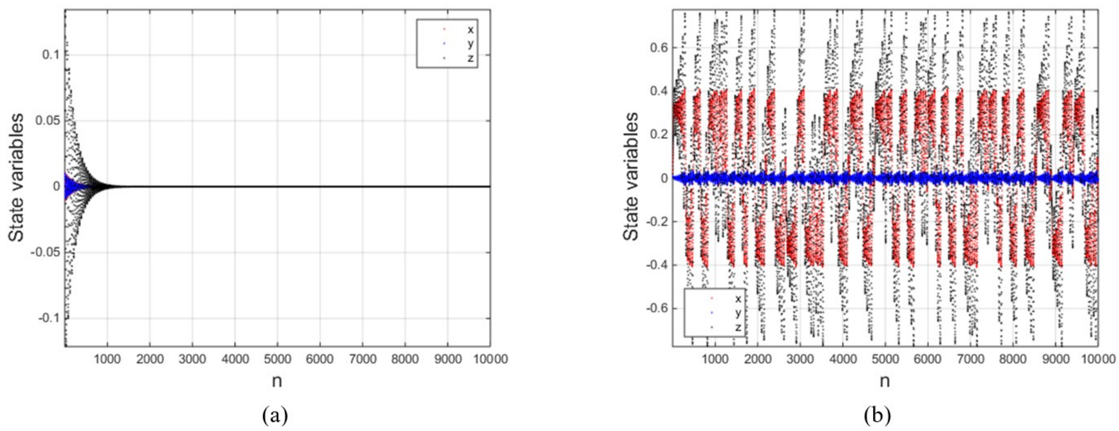

Figure 15: The state variables of the discrete-time MAVPDO *(14)*: (a) are controlled to $\overline{P}_0$ when the FCGs $K_1 = 1$, $K_2 = 0$, and $K_3 = 0$ are implemented, and (b) become chaotic when the FCGs are removed.

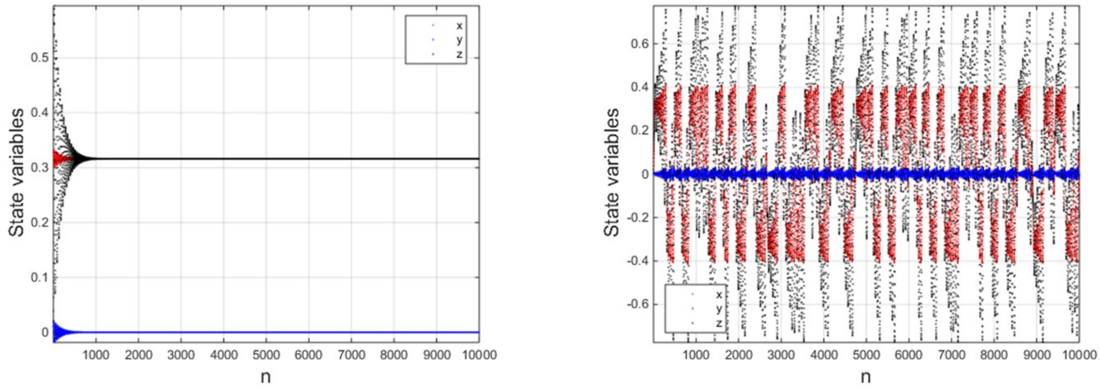

(a) (b)

Figure 16: The state variables of the discrete-time MAVPDO *(14)*: (a) are controlled to $\overline{P}_+$ when the FCGs $K_1 = 1$, $K_2 = 0$, and $K_3 = 0$ are implemented, and (b) become chaotic when the FCGs are removed.

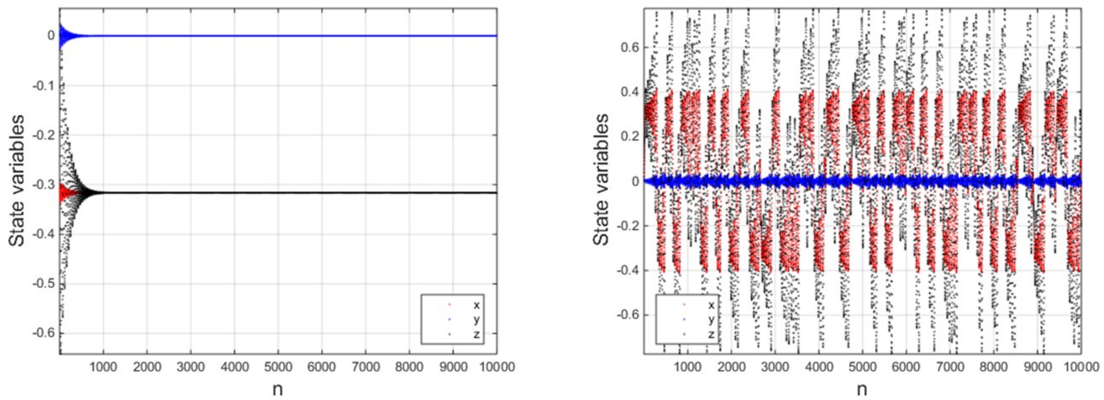

(a) (b)

Figure 17: The state variables of the discrete-time MAVPDO *(14)*: (a) are controlled to $\overline{P}_-$ when the FCGs $K_1 = 1$, $K_2 = 0$, and $K_3 = 0$ are implemented, and (b) become chaotic when the FCGs are removed.

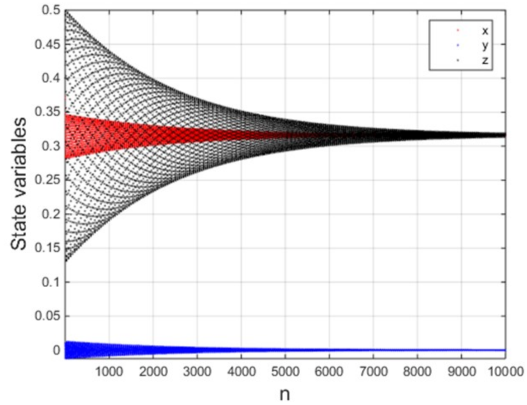

(a) (b)

Figure 18: The state variables of the discrete-time MAVPDO *(14)*: (a) are controlled to $\overline{P}_+$ when $(x_0, y_0, z_0) = (0.4, 0.01, 0.4)^T$ near the blue chaotic attractors (a) than when they are chosen as $(x_0, y_0, z_0) = (-0.4, 0.01, -0.4)^T$ near the red chaotic attractor (b). The FCGs are chosen as $K_1 = 0.181$, $K_2 = 0$, and $K_3 = 0$.

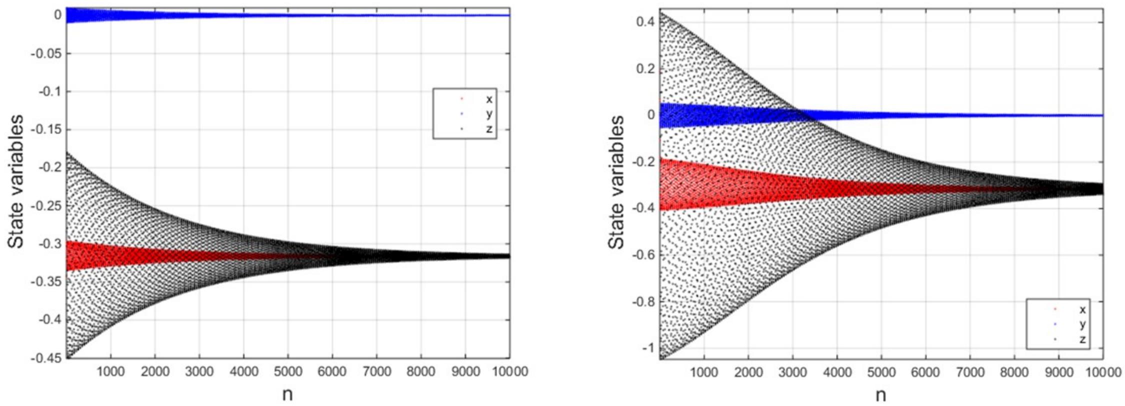

(a) (b)

Figure 19: The state variables of the discrete-time MAVPDO *(14)*: (a) are controlled to $\overline{P}_-$ when $(x_0, y_0, z_0) = (-0.4, 0.01, -0.4)^T$ near the red chaotic attractors (a) than when they are chosen as $(x_0, y_0, z_0) = (0.4, 0.01, 0.4)^T$ near the blue chaotic attractor (b). The FCGs are chosen as $K_1 = 0.28$, $K_2 = 0$, and $K_3 = 0$.

7. Conclusion

The dynamical system of MAVPDO has been discretized based the on Euler's method. The engineering explanation of the discretized system has been explained by designing the corresponding circuit via MATLAB Simulink. Some dynamical behaviors of the considered discrete-time system have been discussed, such as the local stability of the system's three fixed points and the conditions for the N–S bifurcation. Based on computing the first Lyapunov coefficient, it has been found that the N–S bifurcation type is subcritical. Existence of chaotic dynamics in the studied discrete-time system has also been shown via the N–S bifurcation route. Coexistence of two period-1, period-2, period-4, period-5 LCs and two one-band chaotic attractors have been illustrated. The analytical results have supported by numerical simulations such as computation of the MLEs, a bifurcation diagram, phase plots, and basin of attractions, which verify the occurrence of a variety of complex dynamics in the considered discrete-time engineering model. Finally, the discrete-time MAVPDO has been stabilized at all its fixed points using linear control.

In our future works, some applications to the discrete-time MAVPDO will be presented, such as image encryption, biomedical signal encryption, and synchronization of the discrete-time MAVPDO for secure communication.

Acknowledgements

The authors extend the appreciation to the Deanship of Postgraduate Studies and Scientific Research at Majmaah University for funding this research work through the project number (R-2026-86).

References

[1] S. N. Elaydi. *An Introduction to Difference Equations*. Undergraduate Texts in Math. Springer, New York, 3rd edition, 2005.

[2] L. Edelstein-Keshet. *Mathematical Models in Biology*. McGraw-Hill, 1988.

[3] A. E. Matouk and A. A. Elsadany. Dynamical analysis, stabilization and discretization of a chaotic fractional-order glv model. *Nonlinear Dyn.*, 85:1597–1612, 2016.

[4] A. E. Matouk. Chaos and bifurcations in a discretized fractional model of quasi-periodic plasma perturbations. *Int. J. Nonlin. Sci. Numer. Sim.*, 23(7-8):1109–1127, 2022.

[5] G. Gandolfo. *Economic Dynamics: Methods and models*, volume 16 of *Advanced Textbooks in Economics*. North-Holland, Amsterdam, 2nd edition, 1980.

[6] S. S. Askar and K. Alnowibet. Nonlinear oligopolistic game with isoelastic demand function: rationality and local monopolistic approximation. *Chaos Solit. Fract.*, 84:15–22, 2016.

[7] A. E. Matouk, A. A. Elsadany, and Xin B. Neimark–sacker bifurcation analysis and complex nonlinear dynamics in a heterogeneous quadropoly game with an isoelastic demand function. *Nonlinear Dyn.*, 89:2533–2552, 2017.

[8] R. George, N. Gul, A. Zeb, Z. Avazzadeh, S. Djilali, and S. Rezapour. Bifurcations analysis of a discrete time sir epidemic model with nonlinear incidence function. *Results in Physics*, 38:105580, 2022.

[9] K. S. Al-Basyouni and A. Q. Khan. Discrete-time covid-19 epidemic model with chaos, stability and bifurcation. *Results in Physics*, 43:106038, 2022.

[10] Z. Guiying and A. Ruidi. Application of euler method in discrete dynamic systems. *Curriculum and Teaching Methodology*, 6(12):21–27, 2023.

[11] A. E. Matouk and H. N. Agiza. Bifurcations, chaos and synchronization in advp circuit with parallel resistor. *J. Math. Anal. Appl.*, 341:259–269, 2008.

[12] Q-J. Fan. Horseshoe in a modified van der pol–duffing circuit. *Appl. Math. Comput.*, 210:436–440, 2009.

[13] D. C. Braga, L. F. Mello, and M. Messias. Bifurcation analysis of a van der pol-duffing circuit with parallel resistor. *Mathematical Problems in Engineering*, 2009:Article ID 149563, 26 pages, 2009.

[14] L. Wang and Z. Li. Controlling chaos based on the modified advp model. In *2009 International Conference on Intelligent Human-Machine Systems and Cybernetics (IHMSC 2009)*, volume 1, pages 40–43, Hangzhou, Zhejiang, 2009.

[15] L. Wang and Z. Li. Measurement the frequency of weak sinusoidal signal based on the genetic algorithm. In *2010 Sixth International Conference on Natural Computation (ICNC 2010)*, pages 3597–3600, 2010.

[16] H. Zhao, Y. Lin, and Y. Dai. Hidden attractors and dynamics of a general autonomous van der pol–duffing oscillator. *Int. J. Bifurcat. Chaos*, 24:1450080, 2014.

[17] P. Cai, J-S. Tang, and Z-B. Li. Analysis and controlling of hopf bifurcation for chaotic van der pol–duffing system. *Math. Comp. Applic.*, 19:184–193, 2014.

[18] L-Q. Zhou, Z-M. Zhao, D-G. Huang, and F-Q. Chen. Local dynamics of autonomous van der pol–duffing circuit system containing parallel resistor. In *2017 3rd International Conference on Applied Mechanics and Mechanical Automation (AMMA 2017)*, pages 10–14, 2017.

[19] X. Han, F. Xia, P. Ji, Q. Bi, and J. Kurths. Hopf-bifurcation-delay-induced bursting patterns in a modified circuit system. *Commun. Nonlinear Sci. Numer. Simulat.*, 36:517–527, 2016.

[20] B. Zhang, X. Zhang, W. Jiang, H. Ding, L. Chen, and Q. Bi. Bursting oscillations induced by multiple coexisting attractors in a modified 3d van der pol-duffing system. *Commun. Nonlinear Sci. Numer. Simulat.*, 116:106806, 2023.

[21] M. Lakshmanan and K. Murali. *Chaos in Nonlinear Oscillators: Controlling and Synchronization*. World Scientific, 1996.

[22] G. Wen. Criterion to identify hopf bifurcations in maps of arbitrary dimension. *Phys. Rev. E*, 72:026201, 2005.

[23] Y. A. Kuznetsov. *Elements of Applied Bifurcation Theory*. Springer-Verlag, New York, 2nd edition, 1998.